

OBSERVATION OF LARGE  $CP$  VIOLATION IN THE  $B$ -MESON SYSTEM

STEPHEN L. OLSEN

*University of Hawaii, 2505 Correa Road, Honolulu, HI 96822 USA**E-mail: solsen@phys.hawaii.edu*

## REPRESENTING THE BELLE COLLABORATION

A measurement of the  $CP$  violation parameter  $\sin 2\phi_1$  based on a  $29.1 \text{ fb}^{-1}$  data sample recorded at the  $\Upsilon(4S)$  resonance with the Belle detector at the KEKB asymmetric  $e^+e^-$  collider is reported. One neutral  $B$  meson is fully reconstructed as a  $J/\psi K_S$ ,  $\psi(2S)K_S$ ,  $\chi_{c1}K_S$ ,  $\eta_c K_S$ ,  $J/\psi K_L$  or  $J/\psi K^{*0}$  decay and the flavor of the accompanying  $B$  meson is identified from its decay products. From the asymmetry in the distribution of the time intervals between the two  $B$  meson decay points, we determine  $\sin 2\phi_1 = 0.99 \pm 0.14(\text{stat}) \pm 0.06(\text{sys})$ . Since this value is more than  $6\sigma$  from zero, we can conclude that  $CP$  symmetry is violated in the neutral  $B$  meson system.

## 1 Introduction

Violations of  $CP$  symmetry were first observed in the decays of neutral  $K$  mesons in 1964.<sup>1</sup> In 1973, Kobayashi and Maskawa (KM) proposed a model that attributed  $CP$  violation to an irreducible complex phase in the weak-interaction quark mixing (CKM) matrix.<sup>2</sup> The KM idea was remarkable when it was first proposed because it required the existence of at least six quarks at a time when only three quark flavors ( $u$ ,  $d$ , and  $s$ ) were known. The subsequent discoveries of the  $c$ ,  $b$ , and  $t$  quarks, and the compatibility of the model with the  $CP$  violation seen in the neutral kaon system<sup>3</sup> led to the inclusion of the KM mechanism into the Standard Model, even though it had not been conclusively tested experimentally.

The CKM quark mixing matrix relates the weak-interaction ( $d'$ ,  $s'$  &  $b'$ ) and mass eigenstates ( $d$ ,  $s$  &  $b$ ) of the charge  $-1/3e$  quarks:

$$\begin{pmatrix} d' \\ s' \\ b' \end{pmatrix} = \begin{pmatrix} V_{ud} & V_{us} & V_{ub} \\ V_{cd} & V_{cs} & V_{cb} \\ V_{td} & V_{ts} & V_{tb} \end{pmatrix} \begin{pmatrix} d \\ s \\ b \end{pmatrix}. \quad (1)$$

In the most commonly used representations, the complex phase is confined to the furthest off-diagonal elements:  $V_{ub}$  and  $V_{td}$ .

In 1981, Sanda, Bigi and Carter pointed

out that a consequence of the KM model was that large  $CP$  violating asymmetries could occur in certain decay modes of the  $B$  mesons.<sup>4</sup> These authors pointed out that when a neutral  $B$  meson decays to a  $CP$  eigenstate, the amplitude for the direct decay can interfere with that for the process where the  $B$  meson first mixes to a  $\bar{B}$  meson that then decays to the same  $CP$  eigenstate. This is illustrated in Fig. 1, which shows the leading diagrams for the case where the  $CP$  eigenstate is  $(c\bar{c})K^0$  (here  $(c\bar{c})$  denotes a charmonium state). The  $B \rightarrow \bar{B}$  box section of the lower diagram introduces a factor of  $V_{td}^{*2}$  and, thus,  $\phi_1$ , the phase of  $V_{td}$ ,<sup>5</sup> can be determined from the strength of the interference between the two diagrams. For  $(c\bar{c})K^0$  decays, ambiguities due to strong interactions and other  $CP$  violating effects are expected to be small.

A result of this interference is that at the  $\Upsilon(4S)$  resonance the difference between the  $B$  and  $\bar{B}^0$  decay rates to a  $CP$  eigenstate exhibits a time-dependent  $CP$  violating asymmetry

$$\begin{aligned} A_{CP}(\Delta t) &= \frac{R(B^0 \rightarrow f; t) - R(\bar{B}^0 \rightarrow f; t)}{R(B^0 \rightarrow f; t) + R(\bar{B}^0 \rightarrow f; t)} \\ &= \xi_{CP} \sin 2\phi_1 \sin \Delta m \Delta t, \end{aligned} \quad (1)$$

where  $\xi_{CP}$  is the  $CP$  eigenvalue of the final state eigenmode  $f$ ,  $\Delta m$  is the mass difference

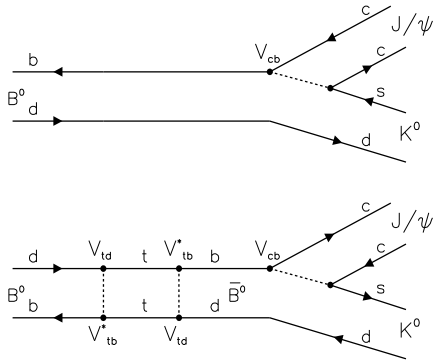


Figure 1. The diagrams for direct (upper) and indirect (lower)  $B \rightarrow J/\psi K^0$  decays. The interference term has a factor of  $V_{td}^{*2}$  from the  $B^0 \bar{B}^0$  mixing box in the lower diagram.

between the two neutral  $B$  meson mass eigenstates and  $t$  is the proper-time interval after the state is defined as either  $B^0$  or  $\bar{B}^0$ . The asymmetry in Eq. (1) vanishes in the time-integrated rate; this is the motivation for asymmetric beam energies in the KEKB collider,<sup>6</sup> which boosts the  $B$  mesons from  $\Upsilon(4S)$  decays and enables a measurement of the time dependence of the decays.

The experimental method for measuring the Sanda-Bigi-Carter asymmetry is illustrated in Fig. 2(a). When the  $\Upsilon(4S)$  decays to  $B^0 \bar{B}^0$ , the two  $B$  mesons are in a coherent  $P$ -wave quantum state. The decay of one of the  $B$  mesons at time  $t_{\text{tag}}$  to  $f_{\text{tag}}$ , a final state that distinguishes between  $B^0$  and  $\bar{B}^0$ , projects the accompanying meson onto the opposite  $b$ -flavor at  $t = t_{\text{tag}}$ ; in this measurement, this meson decays to  $f_{CP}$  at time  $t_{CP}$  (which can be earlier or later than  $t_{\text{tag}}$ ). The manifestation of  $CP$  violation is a time-dependent asymmetry given by  $A(\Delta t)$  of Eq. (1), where  $\Delta t \equiv t_{CP} - t_{\text{tag}}$  is the proper time interval between the decays. For example, if  $\sin 2\phi_1$  is positive, for events where  $f_{\text{tag}}$  is a  $B^0$  and  $\xi_{CP} = -1$  (as is the case for  $f_{CP} = J/\psi K_S$ , the so-called ‘‘golden mode’’), there are more decays with positive  $\Delta t$  values than there are with negative  $\Delta t$  values as indicated in Fig. 2(b); for  $\bar{B}^0$  tags or

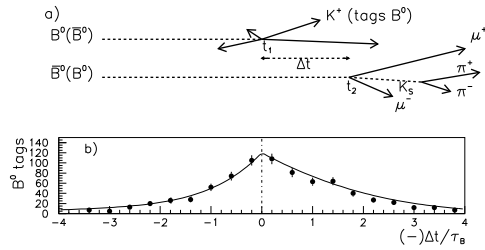


Figure 2. (a) The decay of the upper  $B$  meson to a flavor-tagging state projects the lower  $B$  meson onto the opposite  $b$ -flavor at that time. The interference between the unmixed and mixed decay amplitudes gives rise to a time-dependent asymmetry as indicated in (b).

$\xi_{CP} = +1$  decays, the asymmetry is reversed. As is apparent from Eq. (1), the amplitude of the asymmetry is  $\sin 2\phi_1$ .

Here we report a measurement of  $\sin 2\phi_1$  based on the application of this technique to a data sample that contains 31.3 million  $B\bar{B}$  pairs collected in the Belle detector at the KEKB asymmetric energy  $e^+e^-$  collider. The measurement requires:

- a large sample of reconstructed  $B \rightarrow (c\bar{c})K^0$  eigenstate decays;
- a determination of the flavor of the accompanying  $B$ ;
- a measurement of  $\Delta z$ , the vertex separation between the  $CP$  eigenstate and flavor tag decays; and
- a fit to the flavor-tagged vertex distribution for  $\sin 2\phi_1$ .

## 2 KEKB and Belle

The large sample of  $B$  mesons is produced by KEKB,<sup>6</sup> which is comprised of an 8 GeV  $e^-$  and a 3.5 GeV  $e^+$  storage ring that operate at the  $\Upsilon(4S)$  resonance ( $\sqrt{s} = 10.58$  GeV). The  $\Upsilon(4S)$  and its daughter  $B$  mesons have a boost of  $\beta\gamma = 0.425$  in the laboratory frame that produces a separation between the decay vertices of the two  $B$  mesons,  $\Delta z = z_{CP} -$

$z_{\text{tag}}$ , that is, on average,  $\simeq 200 \mu\text{m}$ ;  $\Delta t$  is determined from  $\Delta z$  via  $\Delta t \simeq \Delta z/\gamma\beta c$ .

KEKB has two special features that minimize the level of background radiation level in the Belle detector: a 22 mrad beam-crossing angle and small beam sizes. The finite beam-crossing angle precludes the need for beam separation dipole magnets in the vicinity of the detector. The interaction-region is arranged so that both the  $e^+$  and  $e^-$  beams each enter the interaction region along the magnetic axis of the final-focus quadrupoles. As a result, the incoming beam particles experience very small transverse quadrupole fields and no dipole field. Because of this, the number of off-momentum beam particles that get swept into the detector is small and the intensity of synchrotron radiation X-rays incident on the portion of the beam-pipe that is exposed to the detector is rather low. Since background levels are a strong function of the beam currents, high luminosity with small beam currents is very desirable. In KEKB the small beam sizes ( $\sigma_y^* \simeq 3\mu\text{m}$ ) have resulted in luminosities as high as  $4.5 \times 10^{33} \text{cm}^{-2}\text{s}^{-1}$  with less than 1 Ampere of current in each beam.

The  $B$  meson decay products are detected and reconstructed in the Belle detector.<sup>7</sup> This is a large solid-angle magnetic spectrometer that consists of a three-layer silicon vertex detector (SVD), a 50-layer central drift chamber (CDC), a mosaic of aerogel threshold Čerenkov counters (ACC), time-of-flight scintillation counters (TOF), and an array of CsI(Tl) crystals (ECL) located inside a 1.7 m radius superconducting solenoid coil that provides a 1.5 T magnetic field. An iron flux-return located outside of the coil is instrumented to detect  $K_L$  mesons and to identify muons. All elements of the detector perform at state-of-the-art levels. Even at the highest luminosities, occupancy levels in all detector components are tolerable and produce no significant deterioration in the performance of any of the detector subsystems.

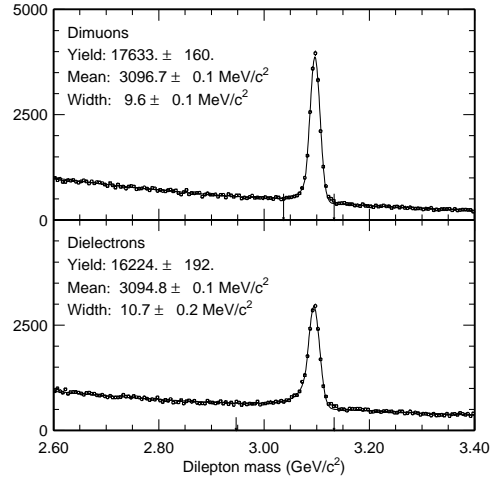


Figure 3. The invariant mass distributions for  $J/\psi \rightarrow \mu^+\mu^-$  (upper) and  $J/\psi \rightarrow e^+e^-$  (lower).

### 3 Selection of $B^0 \rightarrow CP$ eigenstate decays

We reconstruct  $B^0$  decays to the following  $CP$  eigenmodes:<sup>8</sup>  $J/\psi K_S$ ,  $\psi(2S)K_S$ ,  $\chi_{c1}K_S$ ,  $\eta_c K_S$  for  $\xi_f = -1$ , and  $J/\psi K_L$  for  $\xi_f = +1$ . We also use  $B^0 \rightarrow J/\psi K^{*0}$  decays where  $K^{*0} \rightarrow K_S\pi^0$ , where the final state is determined to be an 81 : 19 mixture of  $\xi_f = +1$  and  $-1$  from a fit to the full angular distribution of all  $J/\psi K^*$  decays (other than those with  $K^{*0} \rightarrow K_S\pi^0$ ).

#### 3.1 $B^0 \rightarrow (c\bar{c})K_S$ selection

We reconstruct  $J/\psi$  and  $\psi(2S)$  via their decays to  $\ell^+\ell^-$  ( $\ell = \mu, e$ ). Figure 3 shows the invariant mass distributions for  $J/\psi \rightarrow \mu^+\mu^-$  and  $J/\psi \rightarrow e^+e^-$  after selection. The  $\psi(2S)$  is also reconstructed via  $J/\psi\pi^+\pi^-$ , and the  $\chi_{c1}$  via  $J/\psi\gamma$ . The  $\eta_c$  is detected in the  $K^+K^-\pi^0$  and  $K_S K^-\pi^+$  modes. For the  $J/\psi K_S$  mode we use  $K_S \rightarrow \pi^+\pi^-$  and  $\pi^0\pi^0$  decays; for other modes we use only  $K_S \rightarrow \pi^+\pi^-$ .

Reconstructed charmonium candidates are combined with  $K_S \rightarrow \pi\pi$  candidates to

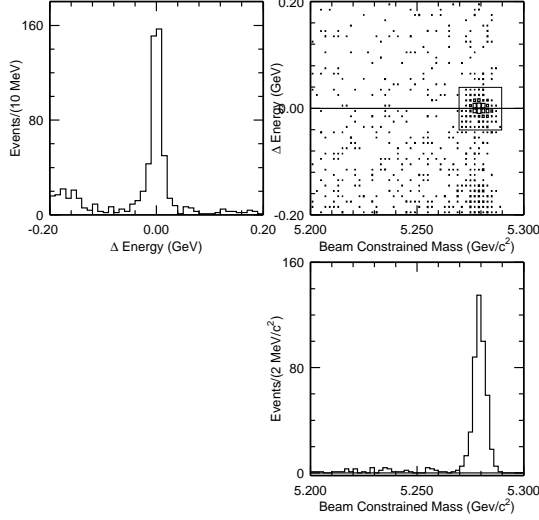


Figure 4. The scatterplot shows  $\Delta E$  vs.  $M_{bc}$  for selected events. The box represents the signal region. The upper left figure is the  $\Delta E$  projection for events in the  $M_{bc}$  signal region; the lower right figure is the  $M_{bc}$  projection for events with  $|\Delta E| < 0.04$  GeV.

form the *energy difference*,  $\Delta E$ , defined as

$$\Delta E \equiv E_{(c\bar{c})} + E_{K_S} - \sqrt{s}/2,$$

where the energies are measured in the center of mass (cm), and the *beam constrained mass*,  $M_{bc}$ , defined as

$$M_{bc} \equiv \sqrt{s/4 - p_B^2},$$

where  $p_B$  is the  $B$  candidate's cm momentum. An  $M_{bc}$  vs.  $\Delta E$  scatterplot for the  $J/\psi K_S$ ,  $K_S \rightarrow \pi^+\pi^-$  candidate events is shown in Fig. 4 together with the projections onto each axis. Candidate  $B$  mesons with  $M_{bc}$  and  $\Delta E$  values within the  $\pm 3.5\sigma$  box (shown in the figure) are selected. For this “golden mode,” there are 457 candidate events with a signal purity of 97%. Candidate events for other  $\xi_f = -1$  modes and for  $J/\psi K^{*0}$  are selected in a similar way. The number of signal-region events and the background levels for each mode are summarized in Table 1.

Table 1. Summary of the number of signal candidates and background level for each CP eigenmode.

Decay mode	$N_{ev}$	$N_{bkgd}$
$B^0 \rightarrow J/\psi K_S$		
$K_S \rightarrow \pi^+\pi^-$	457	11.9
$K_S \rightarrow \pi^0\pi^0$	76	9.4
$B^0 \rightarrow \psi' K_S$		
$\psi' \rightarrow \ell^+\ell^-$	39	1.2
$\psi' \rightarrow J/\psi\pi^+\pi^-$	46	2.1
$B^0 \rightarrow \chi_{c1} K_S$	24	2.4
$B^0 \rightarrow \eta_c K_S$		
$\eta_c \rightarrow K^+K^-\pi^0$	23	11.3
$\eta_c \rightarrow K_S K^-\pi^+$	41	13.6
$B^0 \rightarrow J/\psi K^{*0}(K_S\pi^0)$	41	6.7
Sub-total	747	58.6
$B^0 \rightarrow J/\psi K_L$	569	223

### 3.2 $B^0 \rightarrow J/\psi K_L$ reconstruction

For  $B \rightarrow J/\psi K_L$ , we select events with a  $J/\psi \rightarrow \ell^+\ell^-$  candidate and an isolated neutral cluster in the KLM and/or the ECL that does not match the position of a  $\gamma$  from any reconstructed  $\pi^0 \rightarrow \gamma\gamma$  decay. An example event candidate is shown in Fig. 5, where the  $K_L$  is associated with the cluster of hits in the lower right side of the KLM detector. Using the direction of the centroid of the cluster and the measured  $J/\psi$  four-momentum, we compute the cm momentum of the candidate  $K_L$  for a  $B \rightarrow J/\psi K_L$  two-body decay hypothesis. We reduce backgrounds by means of a likelihood-like quantity that depends on the  $J/\psi$  cm momentum, the angle between the  $J/\psi$  and its nearest-neighbor charged track, the charged-track multiplicity, the extent to which the event is consistent with a  $B^+ \rightarrow J/\psi K^{*+}(K_L\pi^+)$  hypothesis, and the cm polar angle of the reconstructed  $B^0$  meson. In addition, we remove events that are reconstructed as  $B \rightarrow J/\psi K^{(*)}$ , where  $K^{(*)}$  can denote  $K_S$ ,  $K^+$ ,  $K^{*0}(K^+\pi^-, K_S\pi^0)$ , or  $K^{*+}(K^+\pi^0, K_S\pi^+)$ .

Figure 6 shows the  $p_B^* = |p_{J/\psi} + p_{K_L}|$  distribution for selected candidates. Here the



sured particles that distinguish the  $b$ -flavor by the track's charge and/or flavor are selected: high momentum leptons from  $b \rightarrow c\ell\bar{\nu}$ , lower momentum leptons from  $c \rightarrow s\ell^+\nu$ , charged kaons and  $\Lambda$  baryons from  $b \rightarrow c \rightarrow s$ , high momentum charged pions that accompany  $D$  mesons in decays of the type  $B^0 \rightarrow D^{(*)-}(\pi^+, \rho^+, a_1^+, \text{etc.})$ , and slow pions from  $D^{*-} \rightarrow \bar{D}^0\pi^-$ . We use a Monte Carlo simulation to determine a category-dependent variable that indicates whether a particle originates from a  $B^0$  or  $\bar{B}^0$ . The values of this variable range from  $-1$  for a reliably identified  $\bar{B}^0$  to  $+1$  for a reliably identified  $B^0$  and depend on the tagging particle's charge, cm momentum, polar angle, particle-identification probability, as well as other kinematic and event shape quantities. The results from the separate, particle-level categories are then combined in a second stage that takes correlations for the case of multiple particle-level tags into account. This second stage determines two event-level parameters,  $q$  and  $r$ . The first,  $q$ , has the discrete values  $q = +1$  when the tag-side  $B$  meson is more likely to be a  $B^0$  and  $-1$  when it is more likely to be a  $\bar{B}^0$ . The parameter  $r$  is an event-by-event flavor-tagging dilution factor that ranges from  $r = 0$  for no flavor discrimination to  $r = 1$  for unambiguous flavor assignment. The value of  $r$  is used only to sort data into six intervals of flavor purity; the wrong-tag probabilities that are used in the final fit are determined from data.

Reliable values for the incorrect flavor assignment probabilities are essential for the  $\sin 2\phi_1$  measurement. These probabilities,  $w_l$  ( $l = 1, 6$ ), are determined directly from the data for six  $r$  intervals using exclusively reconstructed, self-tagged  $B^0 \rightarrow D^{*-}\ell^+\nu$ ,  $D^{(*)-}\pi^+$ ,  $D^{*-}\rho^+$  and  $J/\psi K^{*0}(K^+\pi^-)$  decays. The  $b$ -flavor of the accompanying  $B$  meson is assigned according to the flavor-tagging algorithm described above. The exclusive decay and the tag vertices are reconstructed using the same vertexing algorithm

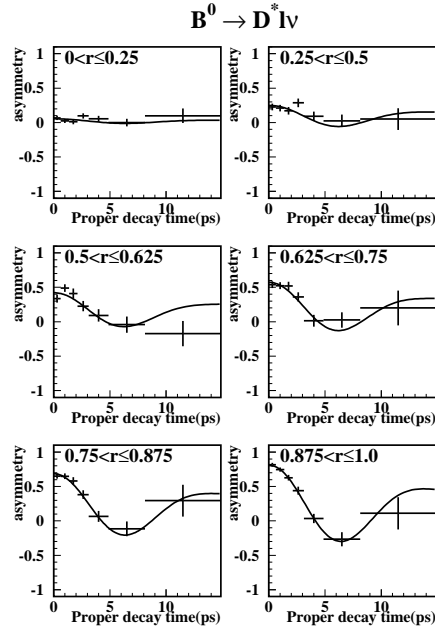


Figure 7. Measured  $(N_{\text{OF}} - N_{\text{SF}})/(N_{\text{OF}} + N_{\text{SF}})$  distributions for the six different  $r$  intervals. The curves are the results of the fits for the incorrect flavor assignment probabilities  $w_l$ . Only the results for the  $D^{*-}\ell^+\nu$  event sample are shown.

that is used to measure the  $CP$  asymmetry as discussed below. The values of  $w_l$  are obtained from the amplitudes of the time-dependent  $B^0\bar{B}^0$  mixing oscillations:  $(N_{\text{OF}} - N_{\text{SF}})/(N_{\text{OF}} + N_{\text{SF}}) = (1 - 2w_l) \cos \Delta m_d \Delta t$ . Here  $N_{\text{OF}}$  and  $N_{\text{SF}}$  are the numbers of opposite- and same-flavor events. The  $B^0\bar{B}^0$  mixing oscillation plots are shown for the six different  $r$  bins in Fig. 7, together with curves that indicate the results of the fits for  $w_l$ . In the fits,  $\Delta m_d$  is fixed at the world average value.<sup>9</sup> Table 2 lists the resulting  $w_l$  values together with the fraction of the events ( $f_l$ ) in each  $r$  interval. The total effective tagging efficiency is  $\sum_l f_l (1 - 2w_l)^2 = 0.270_{-0.012}^{+0.010}$ , where the error includes both statistical and systematic uncertainties.

Table 2. The event fractions ( $f_l$ ) and incorrect flavor assignment probabilities ( $w_l$ ) for each  $r$  interval.

$l$	$r$	$f_l$	$w_l$
1	0.000 – 0.250	0.405	$0.465^{+0.010}_{-0.009}$
2	0.250 – 0.500	0.149	$0.352^{+0.015}_{-0.014}$
3	0.500 – 0.625	0.081	$0.243^{+0.021}_{-0.030}$
4	0.625 – 0.750	0.099	$0.176^{+0.022}_{-0.017}$
5	0.750 – 0.875	0.123	$0.110^{+0.022}_{-0.014}$
6	0.875 – 1.000	0.140	$0.041^{+0.011}_{-0.010}$

## 5 Vertexing

The vertex positions for the  $f_{CP}$  and  $f_{tag}$  decays are reconstructed using tracks that have at least one three-dimensional coordinate determined from associated  $r$ - $\phi$  and  $z$  hits in the same SVD layer plus at least one additional  $z$  hits in the other layers. Each vertex position is required to be consistent with the interaction point profile smeared in the  $r$ - $\phi$  plane by the  $B$  meson decay length. The  $f_{CP}$  vertex is determined using lepton tracks from  $J/\psi$  or  $\psi(2S)$  decays, or prompt tracks from  $\eta_c$  decays. The  $f_{tag}$  vertex is determined from the remaining well reconstructed tracks that are not assigned to  $f_{CP}$ . Tracks that form a  $K_S$  are not used. We use an iterative procedure: if the quality of the vertex fit is poor, the track that is the largest contributor to the  $\chi^2$  is removed and the fit is repeated. The MC indicates that the typical vertex-finding efficiency and vertex resolution (rms) for  $z_{CP}$  ( $z_{tag}$ ) are 92 (91)% and 75 (140)  $\mu\text{m}$ , respectively.

The proper-time interval resolution,  $R(\Delta t)$ , is obtained by convolving a sum of two Gaussians (a *main* component due to the SVD vertex resolution and charmed meson lifetimes, plus a *tail* component caused by poorly reconstructed tracks) with a function that takes into account the cm motion of the  $B$  mesons. The relative fraction of the main Gaussian is determined to be  $0.97 \pm 0.02$  from a study of  $B^0 \rightarrow D^{*-}\pi^+$ ,  $D^{*-}\rho^+$ ,  $D^-\pi^+$ ,  $J/\psi K^{*0}$ ,  $J/\psi K_S$  and  $B^+ \rightarrow \bar{D}^0\pi^+$ ,  $J/\psi K^+$

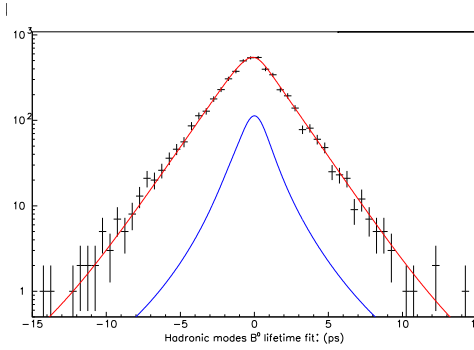


Figure 8. The proper decay time distributions for  $B^0 \rightarrow D^{(*)-}\pi^+$  decays. The upper curve is the result of the fit for the  $B^0$  lifetime; the lower curve represents the background contribution.

events. The means ( $\mu_{\text{main}}$ ,  $\mu_{\text{tail}}$ ) and widths ( $\sigma_{\text{main}}$ ,  $\sigma_{\text{tail}}$ ) of the Gaussians are calculated event-by-event from the  $f_{CP}$  and  $f_{tag}$  vertex-fit error matrices and the  $\chi^2$  values of the fit; typical values are  $\mu_{\text{main}} = -0.24$  ps,  $\mu_{\text{tail}} = 0.18$  ps and  $\sigma_{\text{main}} = 1.49$  ps,  $\sigma_{\text{tail}} = 3.85$  ps. As a verification, we obtain lifetimes for the neutral and charged  $B$  mesons using the same vertexing procedure. Figure 8 shows the  $B^0$  lifetime distribution for reconstructed  $B^0 \rightarrow D^{(*)-}\pi^+$  decays. The fit for the lifetime, shown as the curve in the figure, track the measurements quite well out to nearly  $\pm 10$  lifetimes; the results of the fit agree well with the world average  $B^0$  lifetime value.<sup>10</sup>

After vertexing, 560 events with  $q = +1$  flavor tags and 577 events with  $q = -1$  tags remain. Figure 9 shows the observed  $\Delta t$  distributions for the  $q\xi_f = +1$  (solid points) and  $q\xi_f = -1$  (open points) event samples. Even though this is still “raw data,” i.e. there has been no weighting of events according to their signal purity or flavor-tagging dilution factors, a  $CP$ -violating difference between the two distributions is evident.

We determine  $\sin 2\phi_1$  by performing an unbinned maximum-likelihood fit to the  $\Delta t$  measurements. For modes other than  $J/\psi K^{*0}$ , the probability density function

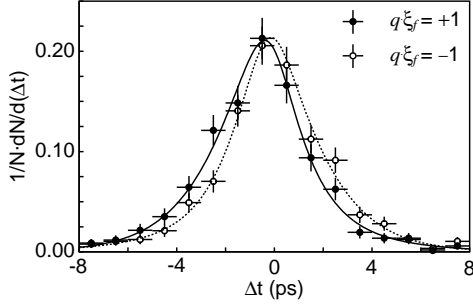


Figure 9.  $\Delta t$  distributions for the events with  $q\xi_f = +1$  (solid points) and  $q\xi_f = -1$  (open points). The results of the global unbinned fit (with  $\sin 2\phi_1 = 0.99$ ) are shown as solid and dashed curves, respectively.

(pdf) expected for the signal distribution is given by

$$\mathcal{P}_{\text{sig}}(\Delta t, q, w_l, \xi_f) = \frac{e^{-|\Delta t|/\tau_{B^0}}}{2\tau_{B^0}} \times \{1 - \xi_f q(1 - 2w_l) \sin 2\phi_1 \sin \Delta m_d \Delta t\},$$

where  $\tau_{B^0}$  and  $\Delta m_d$  are fixed at their world average values.<sup>9</sup> The pdf used for the background distribution is  $\mathcal{P}_{\text{bkg}}(\Delta t) = f_\tau e^{-|\Delta t|/\tau_{\text{bkg}}}/2\tau_{\text{bkg}} + (1 - f_\tau)\delta(\Delta t)$ , where  $f_\tau$  is the fraction of the background component with an effective lifetime  $\tau_{\text{bkg}}$  and  $\delta$  is the Dirac delta function. For all  $f_{CP}$  modes other than  $J/\psi K_L$ , a study using events in the  $\Delta E$  vs.  $M_{bc}$  sideband regions shows that  $f_\tau$  is negligibly small. For these modes we use  $\mathcal{P}_{\text{bkg}}(\Delta t) = \delta(\Delta t)$ .

The  $J/\psi K_L$  background is dominated by  $B \rightarrow J/\psi X$  decays where some final states are  $CP$  eigenstates. We estimate the fractions of the background components with and without a true  $K_L$  cluster by fitting the  $p_B^{\text{cm}}$  distribution to the expected shapes determined from the MC. We also use the MC to determine the fraction of events with definite  $CP$  content within each component. The result is a background that is 71% from non- $CP$  modes with  $\tau_{\text{bkg}} = \tau_B$ . For the  $CP$ -mode backgrounds, we use the signal pdf given above with the appropriate  $\xi_f$  values. For  $J/\psi K^*(K_L \pi^0)$ , which is 13% of the background, we use the  $\xi_f = -1$  content deter-

mined from the full  $J/\psi K^*$  sample. The remaining backgrounds are  $\xi_f = -1$  states (10%) including  $J/\psi K_S$ , and  $\xi_f = +1$  states (5%) including  $\psi(2S)K_L$ ,  $\chi_{c1}K_L$  and  $J/\psi \pi^0$ .

For the  $J/\psi K^*$  mode, we include the  $\Delta t$  and transversity angle  $\theta_{\text{tr}}$  distributions<sup>11</sup> in the likelihood.<sup>12</sup> We use the  $\xi_f$  content determined from the full angular analysis.

Each pdf is convolved with  $R(\Delta t)$  to determine the likelihood value for each event as a function of  $\sin 2\phi_1$ :

$$\mathcal{L}_i = \int \{f_{\text{sig}} \mathcal{P}_{\text{sig}}(\Delta t', q, w_l, \xi_f) + (1 - f_{\text{sig}}) \mathcal{P}_{\text{bkg}}(\Delta t')\} R(\Delta t - \Delta t') d\Delta t',$$

where  $f_{\text{sig}}$  is the probability that the event is signal. The most probable  $\sin 2\phi_1$  is the value that maximizes the likelihood function  $L = \prod_i \mathcal{L}_i$ , where the product is over all events.

The result of the fit is

$$\sin 2\phi_1 = 0.99 \pm 0.14(\text{stat}) \pm 0.06(\text{syst}).$$

In Fig. 10(a) we show the binned asymmetries for the combined data sample that are obtained by applying the fit to the events in each  $\Delta t$  bin separately and then multiplying by the weighted average of  $\Delta m \Delta t$  for that bin. The smooth curve is the result of the global unbinned fit.

Figures 10(b) and (c) show the corresponding asymmetries for the  $(c\bar{c})K_S$  ( $\xi_f = -1$ ) and the  $J/\psi K_L$  ( $\xi_f = +1$ ) modes separately. The observed asymmetries for the different  $CP$  states are opposite, as expected. The curves are the results of unbinned fits applied separately to the two samples; the resultant  $\sin 2\phi_1$  values are  $0.84 \pm 0.17$  (stat) and  $1.31 \pm 0.23$  (stat), respectively.

The systematic error is dominated by uncertainties of the effects of the tails of the vertex distributions, which contribute 0.04. Other significant contributions come from uncertainties in  $w_l$  (0.03), the resolution function parameters (0.02), and the  $J/\psi K_L$  background fraction (0.02). The errors introduced by uncertainties in  $\Delta m_d$  and  $\tau_{B^0}$  are 0.01 or less.

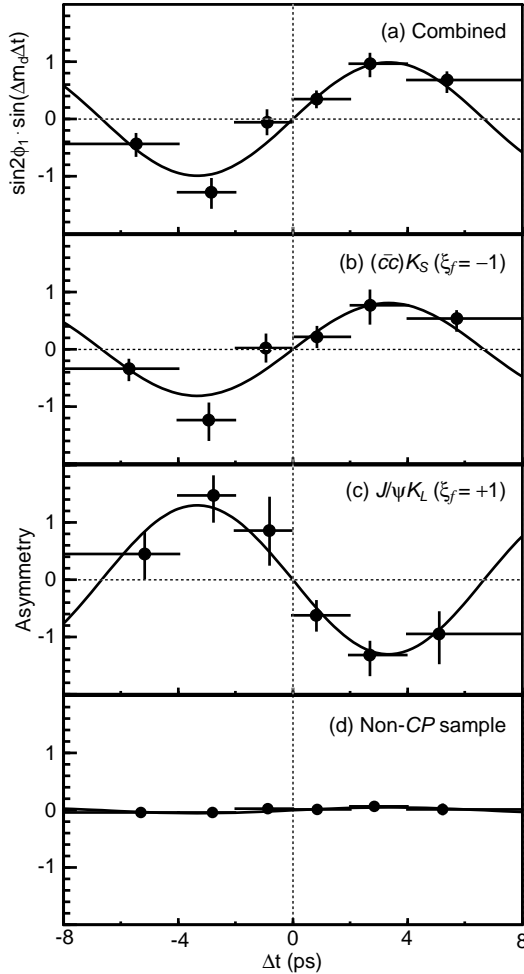


Figure 10. (a) The asymmetry obtained from separate fits to each  $\Delta t$  bin for the full data sample; the curve is the result of the global unbinned fit. (Here,  $-\Delta t$  is used for events with  $\xi_f = +1$ .) Asymmetry plots for the (b)  $(c\bar{c})K_S$  ( $\xi_f = -1$ ), (c)  $J/\psi K_L$  ( $\xi_f = +1$ ), and (d)  $B^0$  control samples are also shown. The curves are the results of unbinned fits applied separately to the individual data samples.

Table 3. The values of  $\sin 2\phi_1$  for various subsamples (statistical errors only).

sample	$\sin 2\phi_1$
$f_{\text{tag}} = B^0$ ( $q = +1$ )	$0.84 \pm 0.21$
$f_{\text{tag}} = \bar{B}^0$ ( $q = -1$ )	$1.11 \pm 0.17$
$J/\psi K_S(\pi^+\pi^-)$	$0.81 \pm 0.20$
$(c\bar{c})K_S$ except $J/\psi K_S(\pi^+\pi^-)$	$1.00 \pm 0.40$
$J/\psi K_L$	$1.31 \pm 0.23$
$J/\psi K^{*0}(K_S\pi^0)$	$0.85 \pm 1.45$
all	$0.99 \pm 0.14$

We performed a number of checks on the measurement. Table 3 lists the results obtained by applying the same analysis to various subsamples. All values are statistically consistent with each other. The result is unchanged if we use the  $w_l$ 's determined separately for  $f_{\text{tag}} = B^0$  and  $\bar{B}^0$ . Fitting to the non- $CP$  eigenstate self-tagged modes  $B^0 \rightarrow D^{(*)-}\pi^+$ ,  $D^{*-}\rho^+$ ,  $J/\psi K^{*0}(K^+\pi^-)$  and  $D^{*-}\ell^+\nu$ , where no asymmetry is expected, yields “ $\sin 2\phi_1'' = 0.05 \pm 0.04$ ”. The asymmetry distribution for this control sample is shown in Fig. 10(d). As a further check, we used three independent  $CP$  fitting programs and two different algorithms for the  $f_{\text{tag}}$  vertexing and found no significant discrepancy.

We conclude that there is large  $CP$  violation in neutral  $B$  meson decay. A zero value for  $\sin 2\phi_1$  is ruled out at a level greater than  $6\sigma$ , which corresponds to less than a part in  $10^7$ . Figure 11 shows the  $1\sigma$  allowed region in the space of KM parameters together with the  $1\sigma$  range of values of  $\phi_1$  from this measurement.<sup>13</sup> Our result is just barely consistent with the higher range of values allowed by the constraints of the KM model as well as with Belle's previous measurement.<sup>14</sup>

## Acknowledgments

We thank the organizers of this conference for inviting us to present our results. We also would like to acknowledge the KEKB accel-

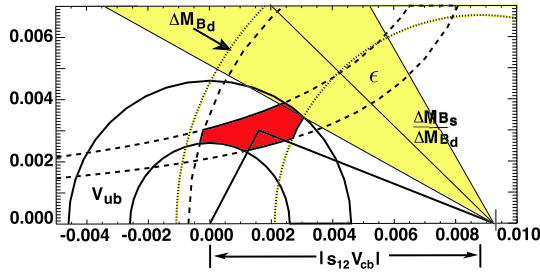


Figure 11. The  $\pm 1\sigma$  region for  $\phi_1$  from this measurement superimposed on the space of CKM matrix parameters. The allowed region that is constrained by other, non- $CP$  measurements is shown as the darker shaded region.

ator group for the excellent operation of the collider.

## References

1. J.H.Christenson et al., Phys Rev. Lett. **13**, 138 (1964).
2. M.Kobayashi and T.Maskawa, Prog. Theo. Phys. **49**, 652 (1973).
3. S. Pakvasa and H. Sugawara, Phys. Rev. **D14**, 305, (1976).
4. A.Carter and A.I.Sanda, Phys. Rev. Lett. **45**, 952 (1980); A.Carter and A.I.Sanda, Phys. Rev. **D23**, 1567 (1981); I.I.Bigi and A.I.Sanda, Nucl. Phys. **B193**, 851 (1981).
5. H. Quinn and A.I. Sanda, Eur. Phys. Jour. **C15**, 626 (2000). (This angle is also known as  $\beta$ .)
6. KEKB B Factory Design Report, KEK Report 95-1, 1995, unpublished.
7. K. Abe *et al.* (Belle Collab.), *The Belle Detector*, KEK Report 2000-4, to be published in Nucl. Instrum. Methods.
8. Throughout this report, whenever a mode is quoted the inclusion of the charge conjugate mode is implied.
9. D.E. Groom *et al.* (Particle Data Group), Eur. Phys. J. **C15**, 1 (2000).
10. The measured  $B$ -lifetimes are:  $\tau_{B^0} = 1.547 \pm 0.021$  ps and  $\tau_{B^+} = 1.641 \pm 0.033$  ps (statistical errors only).
11.  $\theta_{tr}$  is defined as the angle between the  $\ell^+$  direction in the  $J/\psi$  rest frame and the  $z$ -axis, where the  $x$ -axis is defined as the direction of motion of the  $J/\psi$  in the  $\Upsilon(4S)$  rest frame. The  $x$ - $y$  plane is defined by the  $K^*$  decay products in the  $J/\psi$  rest frame.
12. K. Abe *et al.* (Belle Collab.), *Measurements of Polarization and CP Asymmetry in  $B \rightarrow J/\psi + K^*$  decays*, paper submitted to this meeting; BELLE-CONF-0105.
13. In extracting  $\phi_1$  from  $\sin 2\phi_1$ , there is a two-fold ambiguity; for our measurement, the solutions are:  $\phi_1 = 40.9_{-12.5}^{+4.1}$  and  $49.1_{-4.1}^{+12.3}$  degrees. Since the two  $1\sigma$  regions abut, the figure shows  $45^\circ \pm 16.6^\circ$ .
14. A. Abashian *et al.* (Belle Collab.), Phys. Rev. Lett. **86**, 2509 (2001).

## Question

**Don Groom, LBNL:** The asymmetry as you define it lies between  $\pm 1$  and satisfies binomial statistics. What do you mean when you quote something like  $\sin 2\phi_1 = 0.99 \pm 0.14$ ?

**Answer:** In fact, we measure the amplitude of the asymmetry distribution and not the sine of an angle. This amplitude, which is called  $\sin 2\phi_1$  in the context of the KM model, can exceed the  $\pm 1$  "bounds" because of statistical fluctuations or a failure of the model.